Nanoparticle Adhesion and the Role of Nanobubbles in

Single-Particle Collision Electrochemistry

Todd H. Lewis and Bo Zhang*

Department of Chemistry, University of Washington, Seattle, WA, 98195-1700 United States

Corresponding Author: zhangb@uw.edu

Fax: (1) 206-685 8665

Phone: (1) 206-543 1767

Abstract.

Herein, we report how the collision and electrocatalytic behavior of single platinum NPs can be affected by

the transient formation of H₂ nanobubbles generated from the hydrogen evolution reaction (HER). The use

of high concentration acid (0.5 M HClO₄) promotes the nucleation of small nanobubbles, allowing us to

observe a dramatic decrease in the collision frequency. Adding surfactant molecules and a defoaming agent

to the acid solution causes the collision frequency to further decrease and increase, respectively. These

observations support our hypothesis about the critical role of the nanobubble in NP adhesion. Our study

further reveals the complex chemical nature of the electrode/NP system and the interesting role of

transiently formed gas nanobubbles in determining the adhesion probability of individual NPs on an

electrode surface.

Keywords: Nanobubbles, transient detection, electrocatalytic amplification, nanoparticle adhesion,

collision frequency

1

Introduction

The past two decades have seen an increasing interest in studying and further understanding the transient electrochemical and electrocatalytic responses of single nanoparticles (NP) on the surface of an ultramicroelectrode (UME) since the seminal work of Lemay¹ and the following work of Bard². Despite many exciting progresses in the past two decades,³ we have been unable to see much use of the collision principle in practical applications. A significant gap has been our inability to fully understand and control the dynamic and complex collision and electrochemical behavior of single nanoparticles. Herein, we examine the transient collision and electrocatalytic response of single Pt NPs for the hydrogen evolution reaction (HER) at the electrode/solution interface. We were especially interested in understanding the key role of *NP adhesion* in their electrocatalytic behavior. Except for a few special cases,⁴⁴6 the shape of the current signal in Electrocatalytic Amplification (EA)-based NP collision has been described as a stair-shape current response following NP's collision on the electrode. As previously reported by our group, 7 the characteristic peak shape of Pt NPs colliding on a carbon UME in an acid solution is highly potential dependent with sharp ultra-fast spikes predominating at low driving potentials. At higher potentials, the sharp spike is followed by a more steady-state current response with the former being attributed to the formation of a monolayer of adsorbed hydrogen and the latter being attributed to the sustained HER process.

Using a gold UME as their recording electrode, the Sepunaru group further extended these findings⁷ noting the absence or greatly diminished hydrogen adsorption spikes at -0.75V.⁸ Notably, they propose that, due to hydrogen production from their partially active gold electrode, hydrogen gas saturates the surface of Pt NPs prior to collision such that these particles can immediately commence with H₂ production without the H-adsorption step. Interestingly, we observe collision responses similar to that reported by the Sepunaru group but on a carbon electrode at high negative potentials and much higher acid concentration conditions (*vide infra*). We explain such observations based upon the changing kinetics of H-adsorption and HER at different potentials as well as in the context of instrumentation response time limitations.

In addition to peak shape response, we have observed a significant decrease in NP collision frequency at higher negative potentials, e.g., <-0.8 V vs Ag/AgCl, and suggest such a decrease to be due to

the possible formation of the H₂ nanobubbles at the NP's contact point on the electrode surface. The formation of such nanobubbles, regardless of their size, could undoubtedly change the motion of the NPs and reduce their adhesion probability on the electrode. This correspondingly limits our ability to effectively detect transient events as well as limits the overall electrocatalytic activity of individual NP to catalyze the reaction of interest when in poor electrical contact with the electrode surface. The result is a disparity between an expected particle collision detection frequency given the number of available NP and their diffusion coefficient in solution.

Originally developed by Xiao and Bard,² the Electrocatalytic Amplification (EA) method allows one to probe the collision and electrocatalytic property of individual NPs with high throughput by examining the change in the faradaic current signal of a recording ultramicroelectrode (UME). The use of a more inert UME (e.g., carbon) allows one to observe the NP's electrocatalytic signal without much interference from the probe electrode biased at a lower applied potential. *Importantly, however, an effective single-NP event using the EA method involves both the collision and subsequent adhesion of an individual NP to the electrode surface*.^{9,10} Further, it is known individual NPs will remain adhered to the electrode surface following each collision event in the EA method.¹¹

The subject of NP collision frequency in EA, however, has been riddled with discrepancies from theory since the first report in 2007.² Under freely diffusing conditions, the frequency at which single entities collide with an electrode surface is given by **eq 1**^{9,10}

$$f_{\text{diff}} = 4D_{NP}C\alpha N_A \tag{1}$$

where f_{diff} is NP's collision frequency, D_{NP} is their diffusion coefficient, C is the particle concentration, a is the electrode radius, and N_A is Avogadro's number. The diffusion coefficient can be determined using the classical Stokes-Einstein diffusion equation presented below:

$$D_{NP} = \frac{k_B T}{6\pi \eta r} \tag{2}$$

where k_B is Boltzmann's constant, T is the absolute temperature, η is the solution viscosity, r is the particle radius. Importantly, the experimentally observed collision frequency has been significantly lower than that

determined by **eq 1**.^{10,12} Reasons typically cited for such a discrepancy often include NP aggregation,^{4,12} colloidal instability, ^{5,13} or the effective NP adhesion to the electrode surface.¹⁰ Importantly, **eq 1** assumes that 100% of NPs effectively collide and adhere to the electrode surface and that the area occupied by the adhered particles is small compared to the total available electrode area.^{9,10} The question then becomes what is causing the poor adhesion.

Using our microjet collision system,⁷ we effectively limit NP aggregation and colloidal instability as common issues when carrying out NP collision studies under strongly acidic conditions relevant to the HER. In doing so, we consider other variables affecting the NP adhesion beyond high acid concentration and electrolyte conditions. As such, we focus on conditions of high HER driving potentials and high proton concentration to specifically consider the possibility of H₂ nanobubble formation during NP collision and its effect on NP adhesion. Through an examination of transient current fluctuations, we propose a mechanism by which NPs and nanobubbles interact at the electrode surface preventing efficient NP adhesion upon collision resulting in diminished frequency of detection.

Experimental

Chemicals and Materials. All chemicals were used as received from their respective manufacturers. Perchloric acid (HClO₄, Sigma-Aldrich, 70%), sodium perchlorate monohydrate (NaClO₄·H₂O, Sigma-Aldrich, >98.0%), ferrocenemethanol (FcMeOH, Sigma-Aldrich, 97%), potassium chloride (KCl, Fisher Scientific, >99%), potassium ferrocyanide (K₄Fe(CN)₆, Sigma-Aldrich, >99%), trisodium citrate dihydrate (Sigma-Aldrich, >99.0%), Tributyl phosphate (TBP, Sigma-Aldrich, >99%), sodium dodecyl sulfate (SDS, Sigma-Aldrich, >99%), citrate-capped Pt NPs with a diameter of 52 ± 7 nm dispersed in 2 mM sodium citrate (nanoComposix). Although citrate capped NPs were used in all experiments, we neglect their effect on NP adhesion as well as interference with hydrogen adsorption for evidence has previously been reported that citrate anions will be replaced by the dissociated hydrogen atoms on the NP surface at potentials even lower than those considered in this experiment. ¹⁴ It is further known that adsorbed citrate anions can be easily removed from Pt surfaces by cycling the electrode in HClO₄ at low potentials. ¹⁵ All solutions were

prepared with 18.2 M Ω ·cm deionized water from a Barnstead NANOpure water purification system (Thermo Scientific). Perchloric acid solutions tested were of 10 mM and 500 mM bulk concentration. 50 μ M SDS and 1 ppm TBP were used for surfactant and defoaming agent studies, respectively. All solutions intentionally contained higher levels of electrolyte at 100 mM NaClO₄ as a demonstration of the NP aggregation limiting abilities of our pressure-driven microjet collision system.

Fabrication and Characterization of CFEs and Micropipettes. Carbon-fiber microelectrodes (CFEs) were prepared as previously done by our group. ¹⁶ Briefly, a 5-μm-diameter carbon fiber (Besfight G40–800) was aspirated into a piece of glass capillary (1.2 mm O.D./0.69 mm I.D., Sutter) and pulled into two separate tips on a Sutter P-97 puller. Excess carbon fiber protruding from the electrode tip was cut until flush with the pulled glass tip using a scalpel. The tip was then dipped in epoxy (Epo-Tek 301) for 10 min. Silver epoxy (Dupont) was used to connect a tungsten wire to the fiber inside the pipet and Loctite 0151 hysol epoxy adhesive was used to hold the tungsten wire in place. The electrodes were then allowed to set at 80°C each for 2 h. Electrodes were beveled to a 45° angle using a home-built microelectrode beveler. CFEs were characterized using cyclic voltammetry from -0.5 to 0.6 V at 100 mV/s versus Ag/AgCl in 1 mM FcMeOH and 100 mM KCl (Figure S1). Glass micropipettes of ~4 μm diameter orifice were prepared by pulling borosilicate glass capillaries (1 mm O.D./0.5 mm I.D., with filament; Sutter, BF100-50-10) on a P-97 puller as previously reported? with some modification. All potentials are reported verses the Ag/AgCl reference electrode. Only electrodes with a stable voltametric response were used in amperometric experiments. Further, a freshly polished surface was exposed by beveling the CFEs before and after each collision recording.

Microjet Collision System. A Petri dish containing bulk acid solution concentrations at 0.01 M and 0.5 M HClO₄ with 100 mM NaClO₄ was placed on an Olympus IX71 inverted microscope stage. A micropipette was filled with stock concentration 50 nm Pt NPs (0.052 mg/mL), connected to a Femtojet microinjector (Eppendorf), and attached to a micropositioner such that the orifice was dipped in the acid and positioned at a 45° angle. The CFE was then connected to a separate micropositioner directly opposite from the micropipette. The position of the micropipette and the electrode were adjusted until both were in focus

using a 20× objective (0.4 NA Olympus LCPlanFl) and were approximately 5 µm apart facing each other. A constant pressure of 1.3 PSI was applied with a constant 5 µm pipet-electrode distance throughout all experiments. To consider the displacement of acid from the ejected NP and citrate solution, the effective acid concentration at the electrode surface was found to be 8.7% of the bulk concentration under these pressure and distance conditions. This was determined in a similar fashion to our prior work. Briefly, the freely diffusing steady-state response of a 5 µm CFE was determined in bulk 700 mM ferrocyanide with 50 mM KCl as shown in Figure S2A. Selecting a potential of 1.1 V within the steady-state region of the voltammetric response, the 5 µm CFE was connected to the micropositioner and placed directly opposite from a micropipette prepared as described above but filled with 2 mM trisodium citrate dihydrate rather than Pt NP stock solution. The same conditions employed in all other collision experiments were used with output pressure of 1.3 PSI and 5 µm spacing between the citrate-filled micropipette. Both the pipette and electrode were lowered into a Petri dish containing bulk 700 mM ferrocyanide with 50 mM KCl. As shown in Figure S2B, the amperometric current reading yielded a 45 nA steady-state response, or 8.7% of the 520 nA current recorded voltammetric under freely diffusing conditions revealing the effective electrode surface concentration of redox analyte available as a result of pressure-induced displacement. Bulk acid concentration considered in this work, including: [HClO₄]_{bulk} = 500 mM and 10 mM accordingly yield effective concentrations: [HClO₄]_{eff} = 40 mM and 0.9 mM, respectively, at the electrode surface.

Electrochemical Measurements. The CFE was held at a constant potential ranging from -0.4 to -1.2V using a Chem-Clamp potentiostat (Dagan Corporation). An N=1 (gain =1V/nA) headstage was used unless otherwise noted. The current signal was sampled at 100 kHz using a 1322A digitizer (Axon Instruments) and filtered at 10 kHz with a low-pass Bessel filter. Amperometric data were recorded using Axoscope 10.0 software (Molecule Devices) and analyzed with Clampfit 10.4 (Molecular Devices). To record voltametric data, the constant potential output from the Dagan was connected to a Princton Applied Research Corporation (PARC) 175 waveform generator. The current verses potential response was recorded using a PCI-6251 (National Instruments) card on a Dell PC using in-house LabView 8.5 software (National Instruments). All electrochemical experiments were performed in a grounded Faraday cage.

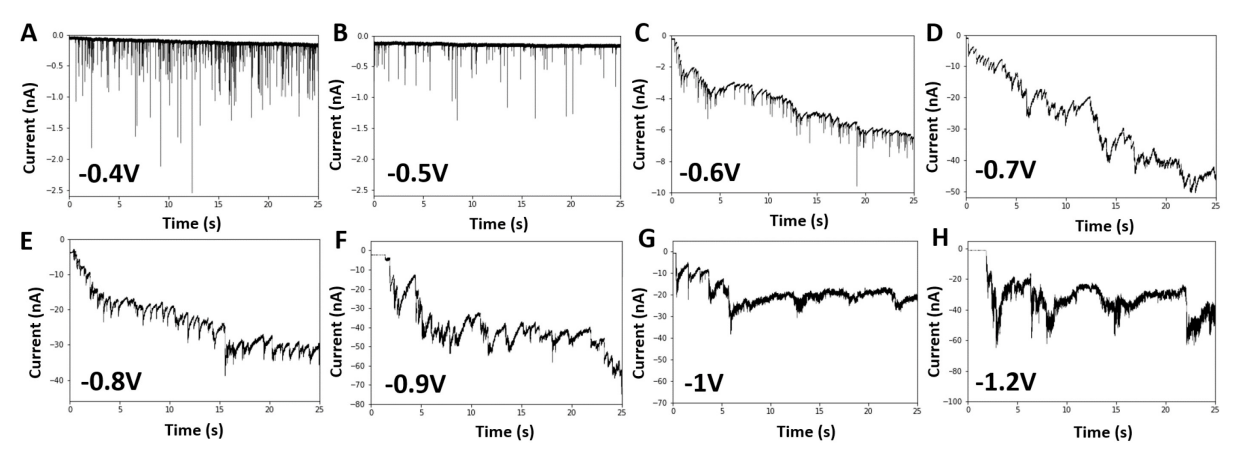


Figure 1. A set of current-time traces illustrating different NP collision behaviors at different applied potentials from -0.4 to -1.2 V. All traces were recorded with 50 nm Pt NPs using a pressure-driven microjet collision system in $[HClO_4]_{bulk} = 0.5$ M, $[HClO_4]_{eff} = 40$ mM (pH = 1.4)

Results and Discussion

Peak Shape of Nanoparticle Collision. Figure 1 displays the characteristic collision and electrocatalytic behavior of individual 50-nm-diameter Pt NPs on the surface of a carbon UME at 0.5 M acid concentration. A Pt NP catalyzes the reduction of protons upon contacting the carbon electrode resulting in a distinct cathodic current peak recorded on the carbon electrode. Depending on the applied potential, tens or even hundreds of well-resolved collision peaks can be readily recorded in most of the 25s recording periods in Figure 1. The use of our micropipette puffing platform⁷ enables us to deliver Pt NPs onto the carbon electrode without significant particle aggregation prior to their collision with the electrode. This allows us to focus our attention on some more extreme reaction conditions, e.g., 0.5 M HClO₄, beyond the limits of traditional EA-based NP collision studies involving the HER.

A clear transition from spike-like collision response to step-like response can be readily seen from **Figure 1** as we increase the voltage driving force for HER. As shown in **Figure 1A,B**, we first observe sharp current spikes on top of a stable current baseline at relatively lower negative potentials, indicating fast reduction of protons ($H^+ + e \rightleftharpoons H_{ads}$) and adsorption of H atoms on the surface of Pt NPs as discussed in our previous study.⁷ This transition can be clearly observed in **Figure 2**, which shows characteristic current spikes recorded at these conditions. The half-width of these H-adsorption spikes usually ranges from 20 to 50 μ s when recorded on a high bandwidth potentiostat⁷ confirming their ultrafast nature. The H-

adsorption process is also self-limiting due to the finite and limited surface area of a single 50 nm Pt NP. Therefore, the reduction current reaches a peak and then quickly drops back to the baseline after the Pt surface is fully covered by a monolayer of H_{ads} atoms.

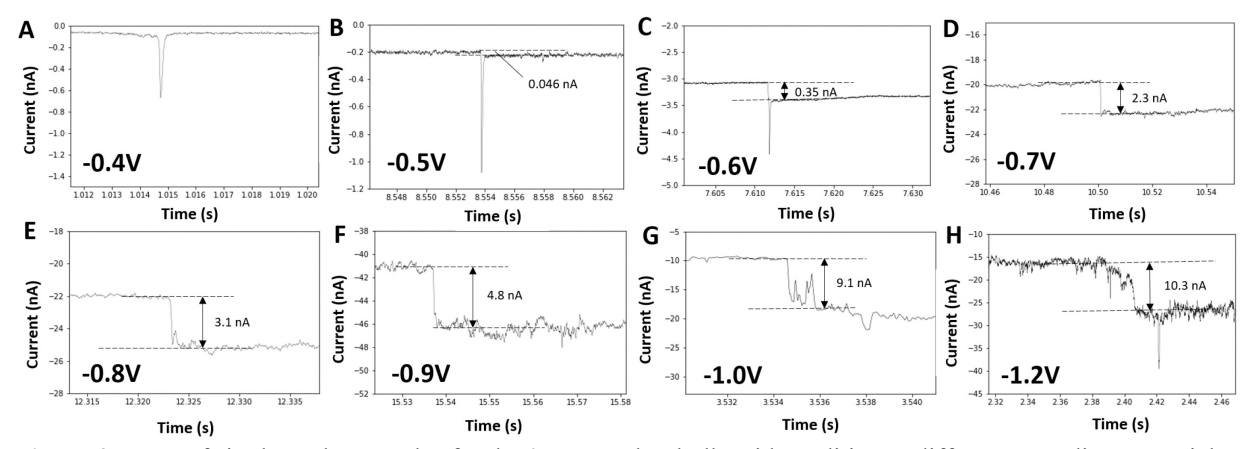


Figure 2. A set of single peak examples for the 0.5 M HClO₄ bulk acid condition at different recording potentials. Notably, a prominent hydrogen adsorption spike is lacking at potentials more negative than -0.6V.

At more negative potentials than -0.4 V, however, one starts to see the appearance of a steady-state reduction wave following the sharp, cathodic current spike (**Figure 2B,C**) suggesting that molecular hydrogen H₂ starts to evolve on the Pt surface at these potentials. Further increasing the negative potential results in an increased HER current relative to the sharp current spikes. Interestingly, at potentials more negative than approximately -0.6 V, it becomes difficult to see the H-adsorption peaks. As shown in **Figure 2D, E, F**, the sharp spike becomes surprisingly absent when the applied potential is more negative than -0.6 V for the 0.5 M acid condition.

Interestingly, the Sepunaru group also observed a lack of an adsorption spike at a similar potential, specifically -0.75V, when they studied Pt NPs on a gold microelectrode in pH = $5.0 (0.01 \text{ mM H}^+)$. They believed that H₂ molecules produced from the partially active gold electrode at -0.75 V saturates the Pt NP surface with surface-adsorbed H_{ads} , prior to the NP's collision with the electrode. As such, although they would still collide on the gold and catalyze HER, their H-adsorption peak would not be detected from the collision response. Although this mechanism is certainly plausible, it is quite unlikely to be the dominating reason for the absent H-adsorption spike in our current study. As one can see from the voltammetry responses of the three electrodes in **Figure 3**, no appreciable HER current can be observed on carbon at

potentials more positive than -1.4 V. As such, it is unlikely a sufficient concentration of H₂ molecules would exist near the surface of the carbon electrode at these potentials.

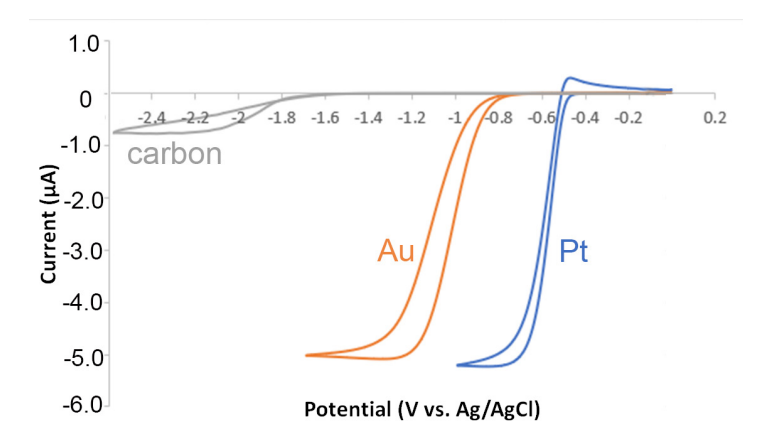


Figure 3. A comparison of the CV response at 100 mV/s for HER on a 25- μ m-diameter Pt (blue), a 25- μ m-diameter Au (orange), and a 5- μ m-diameter CFE (gray).

Herein, we provide another possible mechanism that is more likely to cause the absence of the H-adsorption peaks in our conditions. As illustrated in **Figure 4**, our proposed mechanism has to do with the increasing rates of the two major steps in HER, their competition, and the instrument bandwidth. As reported in our previous study,⁷ the dominating steps in Pt NP-catalyzed HER in this condition are the Volmer step and the Heyrovsky step,

Volmer step:
$$H^+ + e^- \rightleftharpoons H_{ads}$$
 (1)

Heyrovsky step:
$$H^+ + H_{ads} + e^- \rightleftharpoons H_2(g)$$
 (2)

where H^+ denotes protons in the bulk, H_{ads} is surface-adsorbed H atoms, and H_2 (g) is the H₂ molecules evolved from the Pt surface. Upon initial collision, protons are quickly reduced onto the NP surface forming surface-adsorbed H_{ads} atoms. At lower negative potentials (i.e., top panel in **Figure 4**), the Heyrovsky step is kinetically slow allowing the NP to be covered more fully by H_{ads} , and hence, a greater, more detectable spike current can be expected. At higher negative potentials, the Heyrovsky step is significantly faster, which competes with the free H^+ in the vicinity of the Pt NP already absorbed on the carbon at an elevated rate. Therefore, if one is able to take a snapshot of the Pt NP freshly adsorbed on the carbon electrode (i.e., lower panel in **Figure 4**), the Pt surface may only be partially covered by H_{ads} atoms depending on the

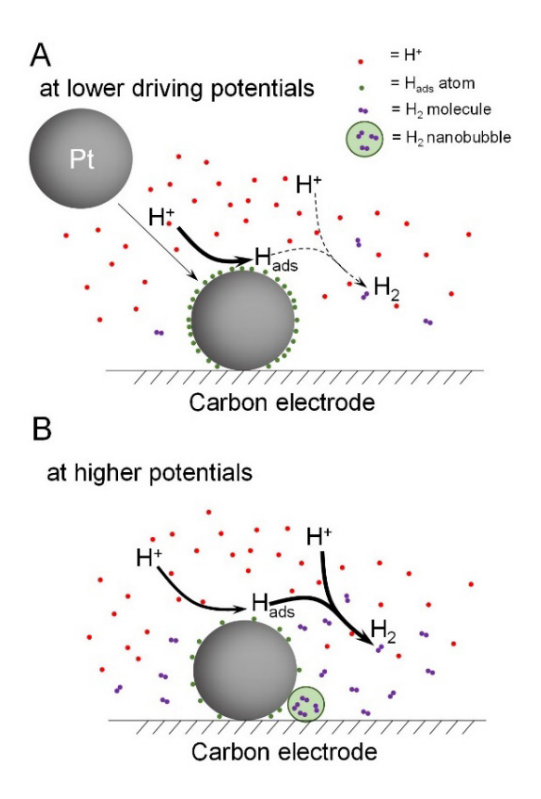


Figure 4. Our proposed mechanism for the reduced cathodic current spikes and the reduced collision frequency.

driving potential, leading to a smaller H-adsorption spike. Another key factor is of course the increased rate of H adsorption with increasing negative potential in combination with instrumental response time limitations, as mentioned in our previous report.⁷ At sufficiently high negative potentials, one can expect that the H-adsorption spike would be indistinguishable from the HER current.

Nanoparticle Collision Frequency. A quick examination of Figure 1 also reveals an interesting decreasing trend to the NP collision frequency as the applied potential was continuously increased in the negative direction. A more quantitative summary of all the collision frequencies is given in Figure 5. All frequencies presented in Figure 5 are tabulated numerically within the Supporting Information within Table S1. There is quite a significant frequency drop (>60%) as the potential was increased from -0.4 V to -0.5 V. In addition, the collision frequency stays relatively constant between -0.5 and -0.8 V. As we further increase the driving potential for HER, however, the frequency drops even more significantly after -0.9 V to less than 1 particles/second. In fact, it becomes somewhat ambiguous to recognize individual NP collision events when more negative potentials were used. Figure S3-S5 provide details for the case of 50-fold

lower acid concentration, specifically: $[HClO_4]_{bulk} = 10 \text{ mM}$, $[HClO_4]_{eff} = 0.9 \text{ mM}$. Importantly, the average collision frequencies observed at 0.01 M bulk acid between -0.4V and -1.0V correlated well with those frequencies observed at 0.5 M between -0.5V and -0.8V suggesting that there is no concentration dependence on collision frequency between 0.01 M and 0.5 M bulk acid at such potentials.

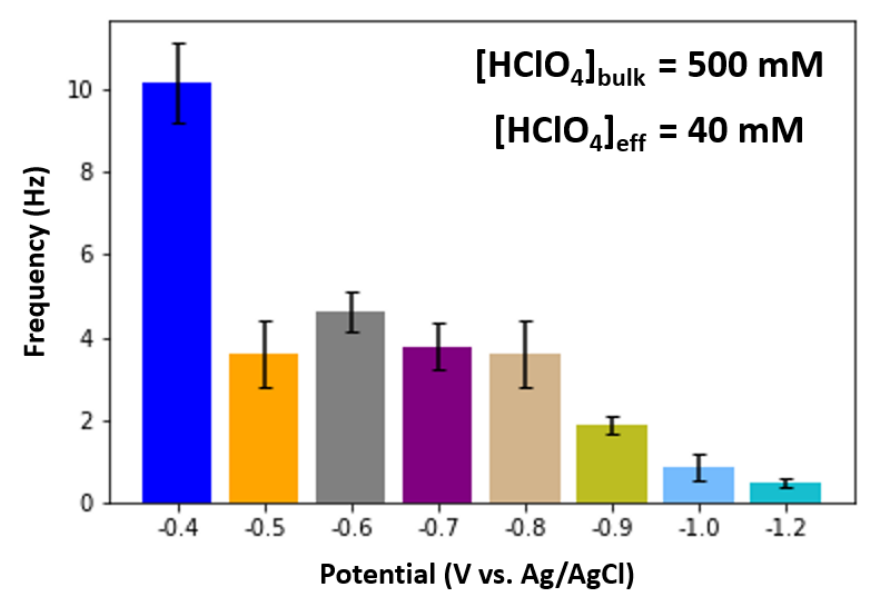


Figure 5. A set of histograms comparing the collision frequencies at different potentials in $[HClO_4]_{bulk} = 0.5$ M, $[HClO_4]_{eff} = 40$ mM at the electrode surface. Frequencies were determined by counting number of collision events within a consistent 25s period of data collection. Error bars represent the standard deviation of n=3 where n is the number of 25s amperometric traces considered.

The more than 2-fold decrease in collision frequency between -0.4 and -0.6 V potentials shown in **Figure 5** was somewhat unexpected and not well understood at this moment. It is worth noting that such a dramatic decrease was only observed at higher acid concentrations. At 10 mM acid concentration, as shown in **Figure S3**, the collision frequency stayed relatively the same between these potentials. It is unlikely that the electrostatic interaction is playing a big role as in both conditions, the solution pH would be less than 2, which is below the pKa = 3.13 of citric acids surface ligands on the Pt NPs.¹⁷ As such, the Pt NPs should be close to neutral and carry no surface charge when they reach the carbon electrode. One hypothesis is that the higher acid concentration and the slower HER rate at lower recording potentials may promote higher H-adsorption signal easier detection of these adsorption events.

Moving into the intermedium potentials, i.e., -0.6, -0.7, and -0.8 V, the collision frequency remains statistically the same at ~3-4 particles/second. Moreover, the individual collision events are easily recognizable in all three conditions despite a changing ratio between the HER steady-state current and the adsorption spike signal. The increasing HER current contributes to a constantly dropping baseline current at higher negative potentials (**Figure 1C-E**).

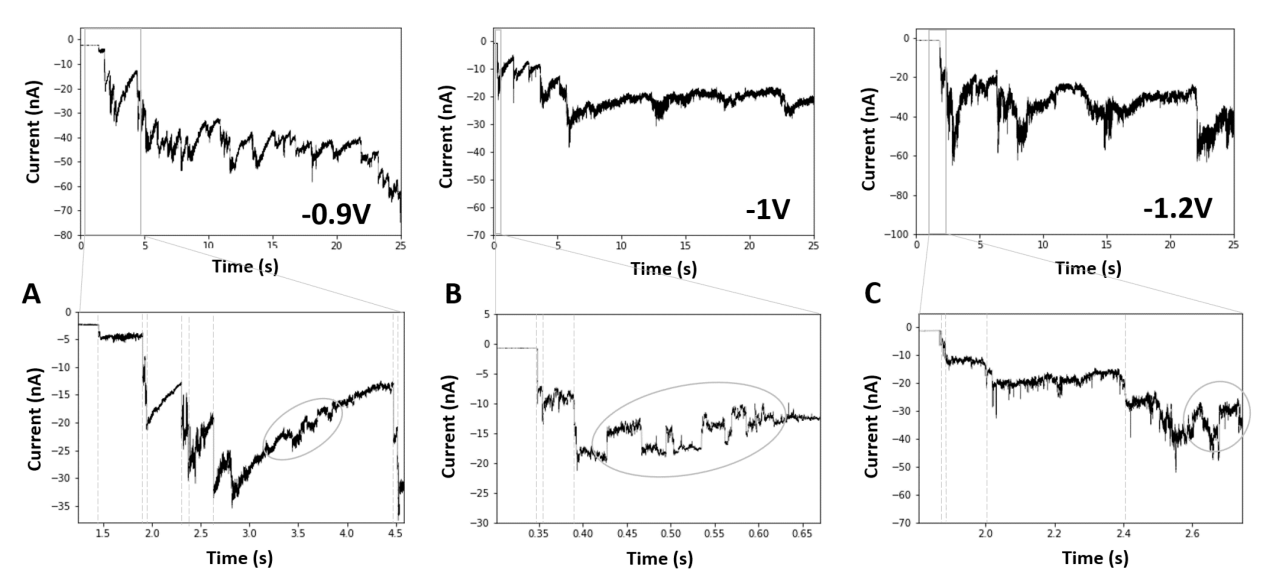


Figure 6. Transient current fluctuations observed with 0.5 M HClO₄ bulk acid: As potentials of **(A)** -0.9V, **(B)** -1.0V, and **(C)** -1.2V. Effective collision signals are indicated by dashed lines while distinct current responses of interest are circled for emphasis.

As we move further to the higher negative potentials, i.e., -0.9 V, -1.0 V, and -1.2 V, the individual collision events become more complex with several interesting aspects noticeable from the recordings in **Figure 1**. First, it becomes more and more difficult to define each collision event from the recorded current-time trace due to the absent adsorption spike and a more fluctuating baseline current prior to each particle collision event. Increased current fluctuations can often be observed following the adhesion of a Pt NP, suggesting particle instability and interesting kinetic NP behavior. In **Figure 6**, we provide a series of representative collision events recorded at these higher negative potentials to further illustrate how catalytic HER current fluctuates with time following a NP collision event.

We highlight these highly fluctuating current responses because we believe they are crucial to our understanding of the significantly decreasing NP collision frequency at potentials more negative than -0.8 V (**Figure 5**). As one can see, many of these current fluctuations within each collision event are rather

similar in magnitude and somewhat random in their spacing on the time axis. The fact that they follow a discrete NP collision event in conjunction with their highly repeatable nature suggests that these fluctuations are due to the same NP making multiple repeated collisions on the same electrode. We believe these repeated NP moves originate from *transient formation of nanobubbles* on the surface of the colliding NP. The rapid, stepwise decrease in current is thought to be due to nanobubble formation, while the rapid increase in current is thought to be due to nanobubble dissolution. Interestingly, these transient current blockades do not return to the pre-collision baseline, indicating that the proposed bubbles to not encapsulate the entire particle, but rather form over a fraction of the NP surface, as illustrated in the right panel of **Figure 4**.

The transient formation and fast dissolution of small nanobubbles is highly possible considering the high acid concentration used in this study. The saturation concentration of H₂ gas in aqueous solution is around 0.8 mM at ambient conditions. 18 Even if only a small fraction of the total acid around the NP is converted to H₂, its local concentration would be well above the saturation point for H₂ leading to possible nanobubble nucleation. If we estimate the theoretical steady-state molecular hydrogen concentration at the surface a single Pt NP on the electrode assuming uniform surface concentration of reaction products (see page S9 of the supporting information), we obtain H_2 concentrations of 27 ± 5 mM, 46 ± 8 mM, and 55 ± 10 10 mM at -0.9V, -1.0V, and -1.2V, respectively, per effective collision event. The combined effect of multiple collision events will only further increase the H₂ content with every subsequent collision supporting an environment favorable to nanobubble nucleation and unfavorable to additional effective NP collision and adhesion with time. A transiently formed nanobubble would undoubtedly be capable of pushing the NP around or causing it to momentarily dislodge or even detach from the carbon surface, especially when the nanobubble is right at the small junction between the NP and the carbon surface. Interestingly, a recent paper by White and coworkers also reported the non-uniform concentration of H₂ around a surface-bound NP and the higher possibility of nanobubble nucleation from the NP-electrode junction.¹⁹

By assuming nanobubbles may be transiently formed and dissolved, we can better understand the decreasing trend in NP collision frequency at potentials more negative than -0.8 V. At such high driving potentials, catalytic HER on Pt NP surface proceed at high rates limited only by proton diffusion. As one can see from Figure 3, the CV response enters into a diffusion limited regime on Pt after reaching ~-0.7 V vs Ag/AgCl in 0.1 M HClO₄. In fact, it is quite possible that H₂O molecules may also start to contribute to some of the cathodic current if the driving potential was further increased. Therefore, it is reasonable to expect that some H2 nanobubbles may quickly nucleate when the Pt NP makes its first contact with the carbon surface. This is especially true if there are already some Pt NP pre-adsorbed on the surface of the carbon UME, which may contribute to an elevated baseline concentration of H₂ in the vicinity of the carbon electrode surface. After all, it requires only 30-60 H₂ molecules to nucleate a small 3-4 nm H₂ bubble as recently suggested by White and coworkers.²⁰ As the formation of such a small number of H₂ molecules only needs ~ 100 electrons (n = 2 electrons for each H₂ molecule), it is unlikely one can detect the faradaic electrical signal associated with it in the current amperometry settings. However, the direct impact of such transient nanobubble formation events is that many of the NP collision events become ineffective events: the particle only makes fast contact with the carbon surface before they are pushed away by the small H₂ nanobubble. It is worth mentioning that nano- or microbubbles have always been utilized to drive the motion of nano- and microparticles in the scientific community. ^{21,22}

Effect of Surfactant and Defoaming Agent

To further test our hypothesis on nanobubbles, we went on and studied the opposite effects of both the addition of a surfactant, sodium dodecyl sulfate (SDS), and a defoaming agent, tributyl phosphate (TBP). As demonstrated by our group, surfactants lower the driving potential needed for nanobubble nucleation by decreasing the surface tension of the gas-water interface.²³ With this in mind, we selected a classic surfactant, SDS, to introduce amphipathic molecules into solution to examine its effect on NP collision frequency. Below pH = 2.5, SDS is known to undergo acid-catalyzed hydrolysis forming 1-dodecanol and HSO_4^- .²⁴ Further, due to the presence of perchlorate, a strong oxidizing agent, 1-dodecanol may be oxidized to either an aldehyde or carboxylic acid.²⁵ Even still, it is presence of such amphipathic

species which is of interest with hydrophilic and hydrophobic moieties lowering gas saturation levels necessary to nucleate nanobubbles. **Figure S6** presents a series of current-time traces similar to that presented in **Figure 1** except with the addition of 50 μM SDS. **Figure 7A** shows the comparison between the NP collision frequencies with and without the addition of 50 μM SDS. Notably, at -0.9 V, the number of effective collision events observed in the SDS-containing solution decreased ~75% compared to the acid only condition. This is also easily noticeable from the raw recordings in **Figure S6** compared to **Figure 1F**. We provide additional examples of highly fluctuating current responses observed in place of successful detection events for both the acid only and SDS conditions within **Figure S7**.

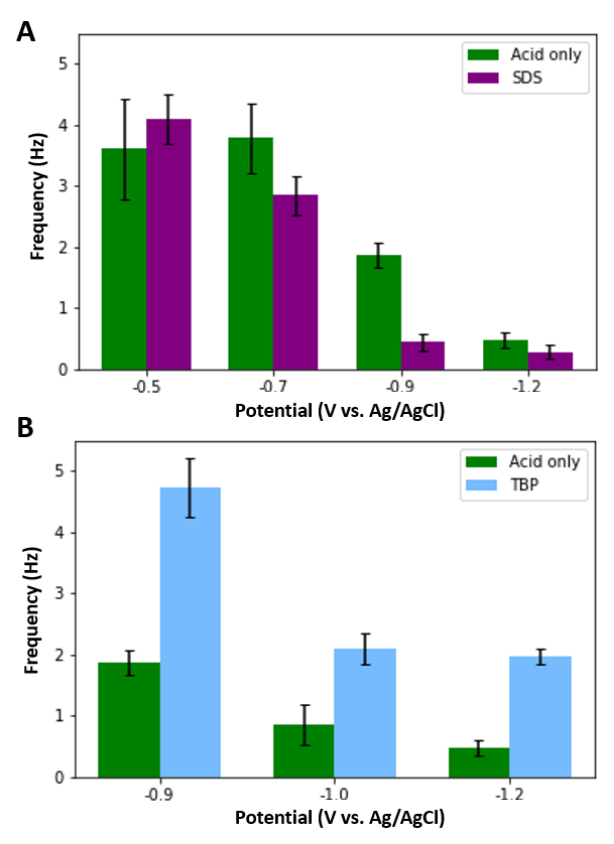


Figure 7. A comparison between collision frequencies and their potential dependence: **(A)** 0.5 M HClO₄ bulk acid with (purple) and without (green) 50 μ M SDS. **(B)** 0.5 M HClO₄ bulk acid with (blue) and without 1 ppm TBP (green). Frequencies were determined by counting number of collision events within a 25s period of data collection. Error bars represent the standard deviation of n = 3 where n is the number of recordings considered.

To further support our claim, we likewise tested the influence of TBP, a defoaming agent. TBP is known to adsorb onto hydrophobic surfaces causing them to become adequately hydrophilic to limit bubble nucleation. Contrary to SDS, the rate of change of dynamic surface tension is known to increase in the presence of TBP. Industrially, TBP is used as a defoaming agent in concert, that has been employed by several research groups involving traditional macroscale bubbles, and it was most recently used by Ma and coworkers in their nanobubble study under acidic (pH = 1.3) conditions. It should be noted that TBP can also undergo acid catalyzed hydrolysis yielding dibutyl phosphate and 1-butanol yet still result in the presence of amphipathic molecules in solution.

Figure 8 presents a series of current-time traces similar to that presented in Figure 1 except with the addition of 1 ppm TBP. Potentials of -0.9, -1, and -1.2 V were selected for the TBP study due to the statistically significant decrease in collision frequency from that observed between -0.5 and -0.8 V in Figure 5. Interestingly, the number of effective collision events observed remarkably increased at all three potentials. Further, the number of repeated current transients observed was notably less or entirely absent when compared to the acid only and SDS condition traces. While baseline noise levels remain high, the baseline levels shown in Figure 8 are fairly consistent with few, if any, sudden periods of amplified current fluctuations. Figure 7B quantitatively confirms the collision frequency increase in the presence of TBP to be statistically significant in comparison to the acid only condition for all potentials considered exhibiting a 2.5, 2.3, and remarkable 4-fold increase at -0.9, -1, and -1.2 V, respectively. Notably, the collision frequency observed at -0.9 V in the presence of TBP in Figure 7B fits within the range of collision frequencies observed between -0.5 and -0.8 V in the acid only condition shown in Figure 5. While the collision at -1.0 and -1.2 V increased considerably in the presence of TBP, consistently elevated baseline noise levels suggest the approach towards water splitting and an activated carbon electrode limiting the possible number of single entity signals observed. It is our ability to both significantly increase or decrease the collision frequency response using surfactant and a defoaming agent which highlights the importance of nanobubble formation, its effect on transient processes, and role at the interface between catalyst and electrode surface.

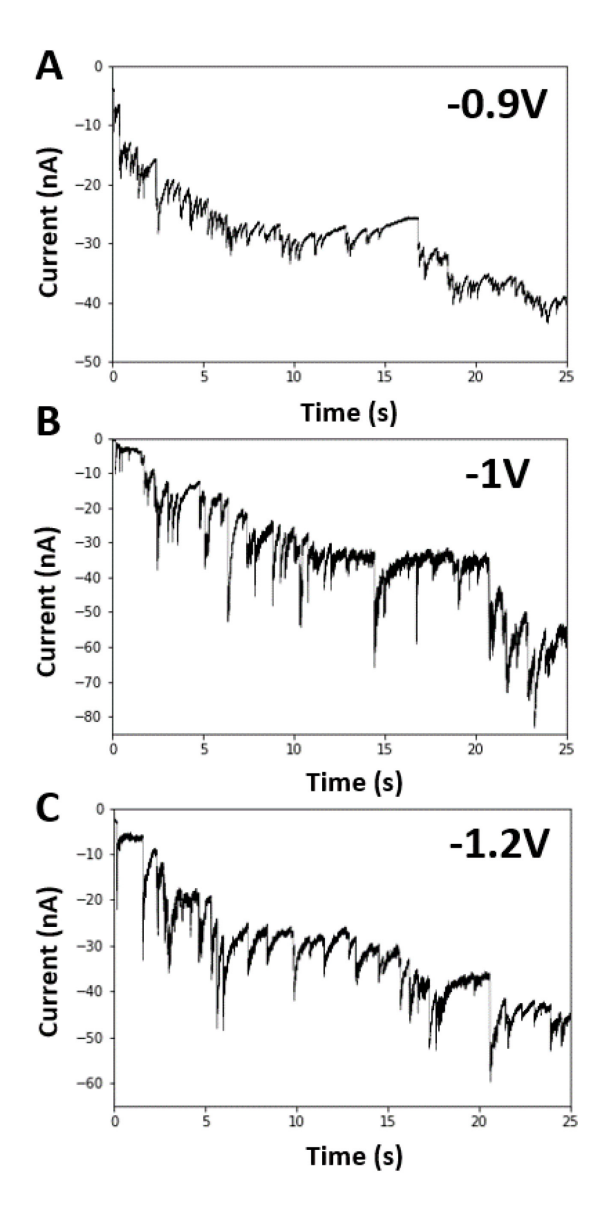


Figure 8. A set of current-time traces illustrating the dependence of NP collision frequency on applied potential in the presence of TBP: **(A)** -0.9 V, **(B)** -1.0 V, **(C)** -1.2 V. All traces were recorded with 50 nm Pt NPs using our pressure-driven microjet collision system in 0.5 M HClO₄ bulk acid with 1 ppm TBP.

Conclusions

In this work, we focused on NP adhesion as a critical factor historically limiting the high throughput nature of NP collision. The use of a glass micropipette allowed us to deliver NPs onto the carbon surface more effectively than in freely diffusing conditions, which enabled us to study NP collision in highly concentrated acid solutions eliminating variables such as aggregation or colloidal instability typically cited

as the cause of diminished single entity detection efficiency. Our results have revealed two interesting dynamic features of NP collision. First, as the driving potential changes for HER, the collision signal changes from a sharp current spike at lower potentials, to a combined spike and step response at intermediate potentials, and to a step only current response observed at even higher potentials. Second, as the negative driving potential increases passing -0.8 V vs Ag/AgCl, the collision frequency decreases significantly compared to lower driving potentials.

We explain the changing peak current response based on the changing kinetics of H-adsorption and HER at different potentials. At lower driving potentials, H-adsorption is the dominating process resulting in a sharp current spike corresponding to the Pt-catalyzed reduction of H^+ and the subsequent formation of a monolayer of H_{ads} on Pt. At higher potentials, however, the HER becomes the dominating process, which competes with the H^+ freely diffusing around the particle. Combined with instrumental bandwidth limitations, this makes it difficult or even impossible to distinguish the charging process from the steady state HER process. We explain the decrease in NP collision frequency at high negative potentials based on the possible formation of a H_2 nanobubble at the contact point between the NP and the carbon electrode. The ability to use a surfactant, SDS and the defoaming agent, TBP to change the collision frequency in two opposite directions further supports our hypothesis.

The direct *operando* imaging of this ultra-fast transient process remains a subject for future work. Simultaneously considering both the transient trajectories of single NPs and the nucleation of nanobubbles at the moment of particle collision remains a challenge. Our work has revealed the complex nature of the dynamic NP collision at the electrode-solution interface and the possible effect of nanobubble formation on NP adhesion on the electrode.

Declaration of competing interest

The authors declare that they have no known competing financial interests or personal relationships that could have appeared to influence the work reported in this paper.

Supporting Information

Potential dependent collision frequency at different conditions, tubulated duration of the hydrogen adsorption spike, CVs of carbon-fiber microelectrode, determination of effective proton concentration at the UME surface, more examples of single collision peaks, calculation of H₂ concentration at the NP surface, more current-time traces at different conditions.

Acknowledgments

The authors gratefully recognize financial support from the National Science Foundation (CHE-2203609). Support from several undergraduate research assistants (Cloris Zhang and Dayna Okazaki) in the carbon-fiber microelectrode fabrication process is further acknowledged. Part of this work was conducted at the Washington Nanofabrication Facility/Molecular Analysis Facility, a National Nanotechnology Coordinated Infrastructure (NNCI) site at the University of Washington with partial support from the National Science Foundation via awards NNCI-1542101 and NNCI-2025489

References

- 1. Quinn, B. M.; Van't Hof, P. G.; Lemay, S. G. Time-Resolved Electrochemical Detection of Discrete Adsorption Events. *J. Am. Chem. Soc.* **2004**, *126*, 8360–8361.
- 2. Xiao, X.; Bard, A. J. Observing Single Nanoparticle Collisions at an Ultramicroelectrode by Electrocatalytic Amplification. *J. Am. Chem. Soc.* **2007**, *129*, 9610-9612.
- 3. Baker, L. A. Perspective and Prospectus on Single-Entity Electrochemistry. *J. Am. Chem. Soc.* **2018**, *140*, 15549-15559.
- 4. Jung, A. R.; Lee, S.; Joo, J. W.; Shin, C.; Bae, H.; Moon, S. G.; Kwon, S. J. Potential-Controlled Current Responses from Staircase to Blip in Single Pt Nanoparticle Collisions on a Ni Ultramicroelectrode. *J. Am. Chem. Soc.* **2015**, *137*, 1762-1765.
- 5. Robinson, D. A.; Kondajji, A. M.; Castañeda, A. D.; Dasari, R.; Crooks, R. M.; Stevenson, K.J. Addressing Colloidal Stability for Unambiguous Electroanalysis of Single Nanoparticle Impacts. *J. Phys. Chem. Lett.* **2016**, *7*, 2512-2517.
- 6. Dasari, R.; Robinson, D. A.; Stevenson, K. J. Ultrasensitive Electroanalytical Tool for Detecting, Sizing, and Evaluating the Catalytic Activity of platinum Nanoparticles. *J. Am. Chem. Soc.* **2013**, 135, 570-573.
- 7. Defnet, P. A.; Han, C.; Zhang, B. Temporally-Resolved Ultrafast Hydrogen Adsorption and Evolution on Single Platinum Nanoparticles. *Anal. Chem.* **2019**, *91*, 4023-4030.

- 8. Roehrich, B.; Sepunaru, L. Nanoimpacts at Active and Partially Active Electrodes: Insights and Limitations. *Angew. Chem. Int. Ed.* **2020**, *59*, 19184-19192.
- 9. Xiao, X.; Fan, F. R. F.; Zhou, J.; Bard, A. J. Current Transients in Single Nanoparticle Collision Events. *J. Am. Chem. Soc.* **2008**, *130*, 16669-16677.
- 10. Kwon, S. J.; Zhou, H.; Fan, F. R. F.; Vorobyev, V.; Zhang, B.; Bard, A. J. Stochastic Electrochemistry with Electrocatalytic Nanoparticles at Inert Ultramicroelectrodes—Theory and Experiments. *Phys. Chem. Chem. Phys.* **2011**, *13*, 5394-5402.
- 11. Ortiz-Ledon, C. A.; Zoski, C. G. Pt Nanoparticle Collisions Detected by Electrocatalytic Amplification and Atomic Force Microscopy Imaging: Nanoparticle Collision Frequency, Adsorption, and Random Distribution at an Ultramicroelectrode Surface. *Anal. Chem.* **2017**, *89*, 6424-6431.
- 12. Kleijn, S. E.; Serrano-Bou, B.; Yanson, A. I.; Koper, M. T. Influence of Hydrazine-Induced Aggregation on the Electrochemical Detection of Platinum Nanoparticles. *Langmuir* **2013**, *29*, 2054-2064.
- 13. Robinson, D. A.; Duay, J.; Kondajji, A. M.; Stevenson, K. J. Mechanistic Aspects of Hydrazine-Induced Pt Colloid Instability and Monitoring Aggregation Kinetics with Nanoparticle Impact Electroanalysis. *Faraday Discuss.* **2016**, *193*, 293-312.
- 14. Xiang, Z.P.; Deng, H.Q.; Peljo, P.; Fu, Z.Y.; Wang, S.L.; Mandler, D.; Sun, G.Q.; Liang, Z.X. Electrochemical Dynamics of a Single Platinum Nanoparticle Collision Event for the Hydrogen Evolution Reaction. *Angew. Chem. Int. Ed.* **2018**, *57*, 3464-3468.
- 15. Zhu, S.; Yue, J.; Qin, X.; Wei, Z.; Liang, Z.; Adzic, R.R.; Brankovic, S.R.; Du, Z.; Shao, M. The Role of Citric Acid in Perfecting Platinum Monolayer on Palladium Nanoparticles During the Surface Limited Redox Replacement Reaction. *J. Electrochem. Soc.* **2016**, *163*, D3040.
- 16. Adams, K. L.; Jena, B. K.; Percival, S. J.; Zhang, B. Highly Sensitive Detection of Exocytotic Dopamine Release Using a Gold-Nanoparticle-Network Microelectrode. *Anal. Chem.* **2011**, *83*, 920-927.
- 17. Traboulsi, H; Awada, C. Toward the Development of Ultrasensitive Detectors for Environmental Applications: A Kinetic Study of Cr(III) Monitoring in Water Using EDTA and SERS Techniques. *ACS Omega* **2020**, *5*, 31352–31361.
- 18. Seo, T.; Kurokawa, R.; Sato, B. A convenient method for determining the concentration of hydrogen in water: use of methylene blue with colloidal platinum. *Med. Gas Res.* **2012**, *2*, 1.
- 19. Georgescu, N. S.; Robinson, D. A.; White, H. S. Effect of Nonuniform Mass Transport on Nanobubble Nucleation at Individual Pt Nanoparticles. *J. Phys. Chem. C* **2021**, 125, 36, 19724–19732.
- 20. German, S. R.; Edwards, M. A.; Ren, H.; White, H. S. Critical Nuclei Size, Rate, and Activation Energy of H₂ Gas Nucleation. *J. Am. Chem. Soc.* **2018**, 140, 11, 4047-4053.
- 21. Mallouk, T. E.; Sen, A. Powering Nanorobots. Sci. Am. 2009, 300, 72-77.
- 22. Paxton, W. F.; Kistler, K. C.; Olmeda, C. C.; Sen, A.; St. Angelo, S. K.; Cao, Y.; Mallouk, T. E.; Lammert, P. E.; Crespi, V. H. Catalytic Nanomotors: Autonomous Movement of Striped Nanorods. *J. Am. Chem. Soc.* **2004**, *126*, 13424-13431.
- 23. Suvira, M. and Zhang, B. Effect of Surfactant on Electrochemically Generated Surface Nanobubbles. *Anal. Chem.* **2021**, *93*, 5170-5176.
- 24. Bethell, D.; Fessey, R. E.; Namwindwa, E.; Roberts, D. W., Hydrolysis of C12 Primary Alkyl Sulfates in Concentrated Aqueous Solutions. Part 1. General Features: Kinetic Form and Mode of Catalysis in Sodium Dodecyl Sulfate Hydrolysis. *J. Chem. Soc., Perkin Trans.* **2001**, *2*, 1489-1495.
- 25. Smith, J. G. Organic Chemistry, 5th ed.; McGraw Hill: New York, 2017.
- 26. Miller, C. A. Antifoaming in Aqueous Foams. Curr. Opin. Colloid Interface, 2008, 13, 177-182.
- 27. Ross, S.; Haak, R.M. Inhibition of Foaming. IX. Changes in the Rate of Attaining Surface Tension Equilibrium in Solutions of Surface-Active Agents on Addition of Foam Inhibitors and Foam Stabilizers. *J. Phys. Chem.* **1958**, *62*, 1260-1264.

- 28. Marklund, A.; Andersson, B.; Haglund, P. Organophosphorus Flame Retardants and Plasticizers in Air from Various Indoor Environments. *J. Environ. Monit.* **2005**, *7*, 814-819.
- 29. Gu, H.; Tang, X.; Hong, R. Y.; Feng, W. G.; Xie, H. D.; Chen, D. X.; Badami, D. Ubbelohde Viscometer Measurement of Water-Based Fe₃O₄ Magnetic Fluid Prepared by Coprecipitation. *J. Magn. Magn. Mater.* **2013**, *348*, 88-92.
- 30. Abedi, M.; Fangueiro, R.; Correia, A. G. An Effective Method for Hybrid CNT/GNP Dispersion and its Effects on the Mechanical, Microstructural, Thermal, and Electrical Properties of Multifunctional Cementitious Composites. *J. Nanomater.* **2020**, *2020*, 1-20.
- 31. Sun, Z.; Gu, Z.; Ma, W. Confined Electrochemical Behaviors of Single Platinum Nanoparticles Revealing Ultrahigh Density of Gas Molecules inside a Nanobubble. *Anal. Chem.* **2023**, *95*, 3613-3620.
- 32. Burger, L. L. *The Chemistry of Tributyl Phosphate: A Review*; NSA-12-005214; General Electric Co. Hanford Atomic Products Operation, Richland, WA, **1955.** https://www.osti.gov/servlets/purl/4334996 (accessed 2023-07-31).

TOC graphic

